Kovove Mater. 59 2021 39–50
DOI: 10.4149/km_2021_1_39

Creep properties of heat-treated Fe-Al-O ODS alloy

S. Fintová, I. Kuběna, M. Jarý, N. Luptáková*, L. Stratil, F. Šiška, J. Svoboda

Institute of Physics of Materials, Czech Academy of Sciences, Žižkova 22, CZ-61662 Brno, Czech Republic

Received 16 October 2020, received in revised form 25 October 2020, accepted 28 January 2021

Abstract

Three different heat treatment regimens were used to modify the microstructure of Fe-Al-O ODS alloy prepared via powder metallurgy. Creep testing at 60 % of alloy state proof stress revealed the highest time to fracture for the bimodal coarse-grained microstructure of the batch heat-treated at 1200 °C for 24 h. Heat treatment at 1100 °C did not significantly influence the creep resistance of the alloy at 60 % of proof stress creep loading. However, the highest creep resistance was achieved by the strongest hindering of dislocations motion, which can be achieved by decreasing the grain size and increasing the density of dispersed particles, which was the case of the basic state material. Creep damage occurred in the specimens' whole volume, and it was characterized by the growth and coalescence of intergranular cavities.

K e y w o r d s: creep, mechanical alloying, powder consolidation, scanning electron microscopy (SEM), electron backscattering diffraction (EBSD)

1. Introduction

Oxide dispersion strengthened (ODS) alloys achieve high strength due to dispersed fine oxides accompanying usual strengthening mechanisms playing a role in conventional alloys (i.e., due to lattice friction, solid-solution, grain boundaries, and secondary particles with coherent and incoherent interfaces) [1, 2]. Usually, the dispersed oxide particles exhibit high thermal stability even at temperatures close to the alloy's melting point and act as barriers to the dislocation's motion during deformation. As a result, a significant improvement of the mechanical properties at elevated temperatures is reached. ODS ferritic steels are known for their good tensile and creep strength at high temperatures with good resistance to swelling, hardening, and embrittlement caused by irradiation [3, 4]. Therefore, they are promising materials for applications such as the 4th generation of fission or fusion reactors, aero-jet turbine blades, etc.

The fine oxide particles are introduced into the material via mechanical alloying. The particles' typical size is between 5–30 nm, and the volume fraction is about 1 % of the material. The mechanical alloying causes homogeneous distribution of these introduced nano-oxides in the metal matrix, while they might be transformed into complex oxides during heat treatment [3–6]. The dispersoid particles interacting with grain boundaries play an essential role in the alloy microstructure stabilization [7]. Usually, Y, La, Ce, Zr, or Mg oxide particles with significantly higher thermodynamical stability, compared to borides or nitrides, are used as the dispersoid particles [8, 9]. Since the grain and particle size can be controlled by heat treatment [3–5, 10, 11], the ODS alloys' properties can be tailored easily. Combination of fine dispersoids with a coarse-grained microstructure of ODS materials stabilized during annealing at high temperatures resulted in a creep resistance significantly higher than that of conventional wrought or cast alloys [4].

The creep behaviour of ODS alloys can be divided into two regions by a specific stress threshold value. At stresses below the threshold value, the creep rate of ODS alloys becomes negligible. The explanation of the observed phenomena is in acting of the dispersed nano-oxides as barriers to dislocation motion. However, it is still not sufficiently explained, why the effect is so intensive [3, 5]. According to [5, 12], the interaction between dislocations and nano-oxides is attractive at high temperatures due to the diffusional relaxation

*Corresponding author: e-mail address: luptakova@ipm.cz

of the dislocation stress field and decreased dislocation line energy at the incoherent particle/matrix interface. Subsequently, significant threshold stress must be overcome to detach dislocations from the attracting particles [5, 13]. While the mechanism of detaching of the dislocations from the nano-oxide particles over the threshold stress value was shown to be assisted with diffusional creep, the dominant creep damaging mechanism was concluded to be dependent on the ODS alloy grain size and strain rate [5].

Fe-Al based alloys combine excellent high-temperature oxidation and corrosion resistance and good mechanical properties with low-cost production and a wide range of processing methods. Such a combination makes them a promising material for structural applications operating at high temperatures, the mechanical properties of which can be significantly enhanced by the dispersion of fine oxide particles.

The present paper is focused on the analysis of creep properties of the Fe-Al-O ODS alloy influenced by microstructural changes due to different heat treatments. The material was prepared from Fe and 11 wt.% of Al powders mechanically alloyed in the oxygen atmosphere. The basic creep resistance is evaluated at 60 % proof stress for individual ODS alloy states as the standard characteristic. The obtained creep properties are linked to the resulting microstructure. The obtained results enhance basic knowledge about the ODS alloy response to the creep damage and predict material long term properties under elevated temperature loading.

2. Experimental material and methodology

2.1. Experimental material processing

Fe-Al-O ODS alloy was prepared via mechanical alloying at IPM. To prepare the experimental material, Fe and Al powders with the purity of 99.9 % (11 wt.% of Al) were used. The powders were mechanically alloyed in the vacuum-tight milling container for four weeks in an oxygen atmosphere, which was consumed. A protective argon atmosphere was adopted during the canning of the prepared powder into the tubular container. The evacuated container was rolled at 900 ℃ to a form of a plate of a thickness of 7 mm. After rolling, the steel container was removed by machining.

Three different heat treatments were used for the alloy annealing. The first batch was subjected to the temperature of 1100 ℃ for 3 h, the second one to the same temperature for 24 h, and the third one to the temperature of 1200 ℃ for 24 h. The heat treatment was conducted in the muffle atmospheric furnace. The specimens were heated up within 10 minutes and cooled down within 5 min.

2.2. Microstructural analysis

Metallographic specimens of the Fe-Al-O ODS alloy states were prepared by conventional procedures including grinding on SiC papers, polishing on diamond paste, and polishing using colloidal silica suspension. The microstructure of individual material states was examined using Tescan LYRA 3 XMU FEG/SEM×FIB microscope (SEM). Back-scatter mode (BSE) was adopted to reveal material microstructure.

The grain size was determined using the electron backscattered diffraction (EBSD) method. The high angle grain boundaries were determined as the misorientation of 10°. The analysis was performed before testing and after creep tests performed under tensile loading of 60 % of proof stress determined at 800 ℃ for each alloy state. At least the area of 80 × 40 μm^2 was analyzed to determine the average grain size of the fine-grained alloy state and 1500 × 1000 μm^2 for the coarse-grained alloy state.

The oxide particles' size was determined from high magnification SEM micrographs and verified by analysis of transmission electron microscopy (TEM) images of alloy states microstructure. ImageJ software was used for the oxide particle size determination from both SEM and TEM micrographs.

Typical microstructures of the Fe-Al-O ODS alloy batches are shown in Fig. 1. The average grain size of 0.4 ± 0.2 μm was characteristic for the basic material (see Fig. 1a). Dispersed oxide particles representing almost 2 % of the area fraction were present in the interior of the grains and at the grain boundaries. Most of the particles were within the size below 20 nm (59 %), 87 % of the present particles had the size below 50 nm.

Annealing at 1100 ℃ for 3 h resulted in slight microstructural changes, see Fig. 1b. The average grain size of 0.4 ± 0.2 μm was characteristic for the alloy state, however, locally, the grain coarsening (up to 5 μm) was observed. Also, the particles coarsening due to the heat treatment was observed (occupy almost 4 % of the area fraction). Only 24 % of the particles were of the size below 20 nm (no particles below 10 nm were detected in the microstructure), and the fraction of particles with a size below 50 nm decreased to 76 %.

Prolongation of the annealing time resulted in a more pronounced local grain coarsening and particles coarsening, see Fig. 1c. The average grain size was 0.45 ± 0.2 μm. The fraction of particles with a size below 50 nm decreased to 70 %, and only 17 % of the particles were of the size below 20 nm (no particles below 10 nm were detected again in the microstructure). The particles occupied almost 4 % of the microstructure area fraction.

Heat treatment at 1200 ℃ for 24 h resulted in the dissolution of small oxide particles and growth of large oxide particles, see Fig. 1d. Still, some areas (below

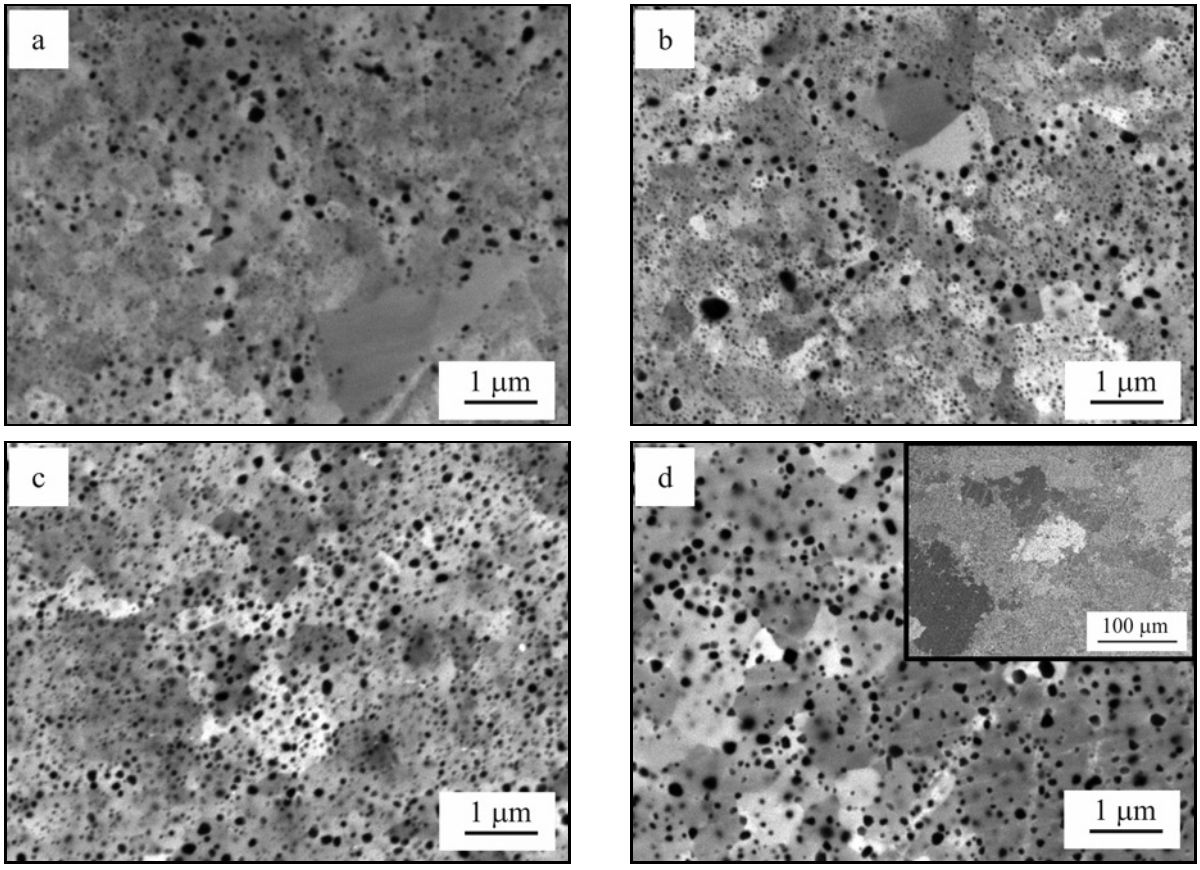

Fig. 1. A typical microstructure of tested Fe-Al-O ODS alloy states, SEM, BSE: (a) basic state, (b) 3 h/1100 °C, (c) 24 h/1100 °C, and (d) 24 h/1200 °C.

Table 1. Tensile properties of the Fe-Al-O ODS alloys tested at 800 °C [14].

Specimen	PS (MPa)	UTS (MPa)	Ductility (%)
Basic state	161	175	11.6
3 h/1100 °C	118	123	24.4
24 h/1100 °C	100	104	29.4
24 h/1200 °C	87	90	25.2

35 % area fraction) with refined grains (average grain size of 0.5 ± 0.4 μm) survived in the microstructure, and the coarse recrystallized grains achieved the average size of 79.7 ± 31.7 μm (macro-view included). In the microstructure, no particles with the size below 20 nm were observed, and the number of particles with the size below 50 nm decreased to 31 %. The number of particles having a size above 100 nm reached almost 17 %. The increase of the area fraction of the particles was observed; the particles occupied nearly 9.5 % of the microstructure area fraction. The reason for the measured increase is discussed in detail in [14].

Tensile properties, i.e., proof stress – PS, ultimate tensile strength – UTS, and ductility for corresponding material states determined at 800 °C are listed in Table 1. PS and UTS decrease with time and temperature of heat treatment. More details are provided in [14].

3. Creep tests

Creep tests were performed on the universal creep testing machine with an electromechanical crosshead, lever arm and spring loading system. Flat specimens with a cross-section of 4 × 3.2 mm^2 and the gauge length of 25 mm were subjected to testing (Fig. 2). Specimens surface was fine-ground using SiC paper up to 1200 grit. The stress axis of the tested specimens was parallel to the rolling direction of the plate. The surface of the tested specimens was fine ground before loading (up to SiC paper no. 2500). The tests

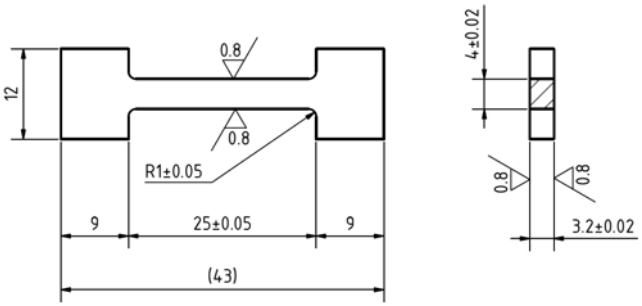

Fig. 2. The geometry of the specimen for creep test. Dimensions are in mm.

were performed at 800 ℃ (1073 K) in a tensile loading mode. Preloading of 1.5 kg was applied for the period of specimen and testing device tempering to the testing temperature. The tests were carried out in a 5N argon atmosphere.

A loading of 60 % of PS determined for the individual alloy states at 800 ℃ was applied for primary material creep properties characterization. Based on the obtained results, two levels of tensile loading, 60 and 90 MPa, were used for further creep testing and the comparison of the individual material states response to the creep loading.

3.1. Creep damage analysis

The analysis of the specimen damage and the fracture surface analysis were performed in terms of scanning electron microscopy using SEM. The microstructure of the specimens was analyzed to reveal the microstructure's influence on the creep loading and its behaviour. Fe-Al-O ODS alloy microstructures of individual batches were related to the obtained creep data.

4. Results and discussion

4.1. Creep tests

Static recrystallization was observed for the Fe-Al-O ODS alloy during the applied heat treatment. The grain growth was significantly pronounced in the case of the higher annealing temperature. Heat treatment also resulted in the coarsening of oxides by the dissolution of small oxides and large oxides' growth (Ostwald ripening). The findings are in agreement with [3, 10, 11]. Microstructure coarsening was corresponding to the temperature and time of the heat treatment applied. Higher treatment time and higher temperature resulted in more pronounced microstructure coarsening, while both the grain size and the particles size were influenced.

The microstructural changes were manifested in the creep resistance of the alloy states. Creep behaviour and the obtained creep characteristics for tested Fe-Al-O ODS alloy batches are shown in Fig. 3. The results of the creep rate vs time are smoothed by splining.

Three different comparisons were performed for the four material states. The influence of the microstructural changes occurring due to heat treatment is summarized in Fig. 4.

The first comparison was performed for the creep at a relative level of tensile loading, corresponding to 60 % of PS. The decrease of tensile properties is in agreement with microstructural changes and follows the literature [4, 11, 15, 16]. The increase of the grain and particle size was accompanied by decreased material strength and an increase of ductility. The drop of ductility in the case of heat treatment at 1200 ℃ for 24 h can be attributed to a very coarse and heterogeneous bimodal grain microstructure. As a consequence, the decreased values of the tensile loading were applied for coarsened alloy states. The results are shown in Figs. 3a,b and summarized in Table 2. The highest time to creep fracture was observed for the batch heat-treated at 1200 ℃ for 24 h, which was more than 10 times longer when compared to other batches, see Table 2. The secondary creep rate value was lower by one order of magnitude for the batch 24 h/1200 ℃. Higher values of the creep ductility were typical for the batches treated at 1100 ℃, while similar values were determined for the basic state and batch heat-treated at 1200 ℃.

The results can be explained by the respective microstructural characteristics. Two main phenom-

Table 2. Creep characteristics of Fe-Al-O ODS alloy states tested under tensile loading of 60 % PS

Specimen	Tensile loading (MPa) (60 % PS)	Time to fracture (h)	Average secondary creep rate (h^{-1})	Creep fracture strain (%)
Basic state	96.6	17.44	5.00×10^{-4}	2.00
3 h/1100 ℃	70.8	20.63	9.00×10^{-4}	3.42
24 h/1100 ℃	60.0	32.49	9.00×10^{-4}	4.97
24 h/1200 ℃	52.2	306.72	3.00×10^{-5}	2.05

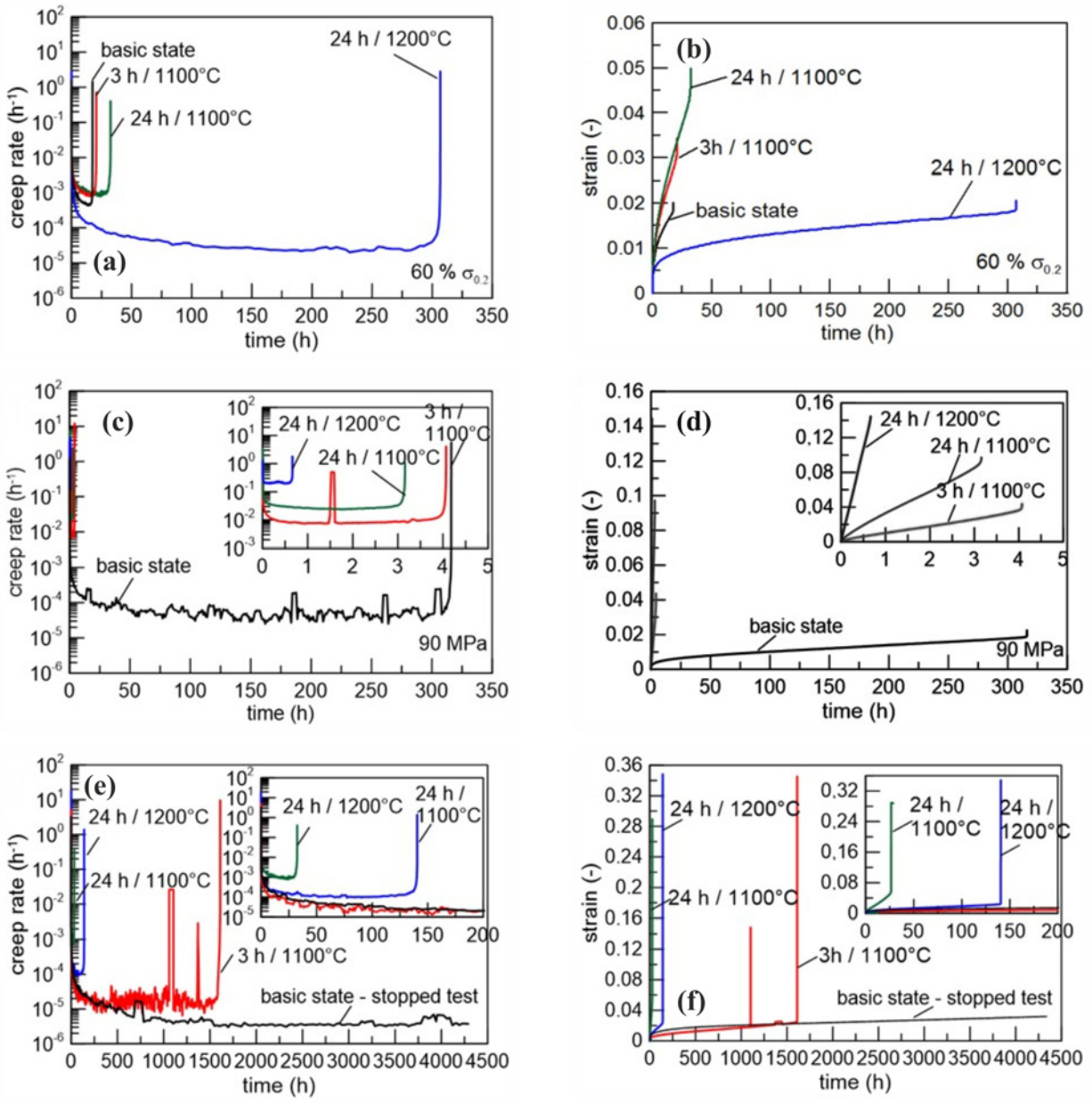

Fig. 3. Creep behaviour of Fe-Al-O ODS alloy tested at 800 °C under tensile loading: (a) creep rate, 60 % PS, (b) creep strain, 60 % PS, (c) creep rate, 90 MPa, (d) creep strain, 90 MPa, (e) creep rate, 60 MPa, and (f) creep strain, 60 MPa.

ena cause creep damage: dislocation motion and mass diffusion dominating at grain boundaries. These two mechanisms lead to the nucleation of cavities, their growth, and coalescence. Dislocations motion is driven by the applied stress and hindered by the dispersed particles, grain boundaries, and dislocation forest. Diffusion is activated by temperature and amount of lattice defects and driven by internal stress gradients. The applied stress was the highest for the basic state and the lowest for the specimens 24 h/1200 °C. Therefore, the basic state with many grain boundaries loaded at the most elevated stress showed the shortest time to fracture while the 24 h/1200 °C batch (low number of grain boundaries, the lowest stress) the longest one. These observations correspond to other studies where large grains present in the microstructure generally result in significantly better creep properties than the microstructures with small grain size, as shown in [4, 11, 17].

To compare the batches, two absolute levels of creep loading were applied to all batches. The first one was set to 90 MPa which represents the value slightly lower than 60 % of PS of the basic material and the second one was 60 MPa which represents the median value of 60 % of PS for the heat-treated materials. The creep results are presented in Figs. 3c–e and

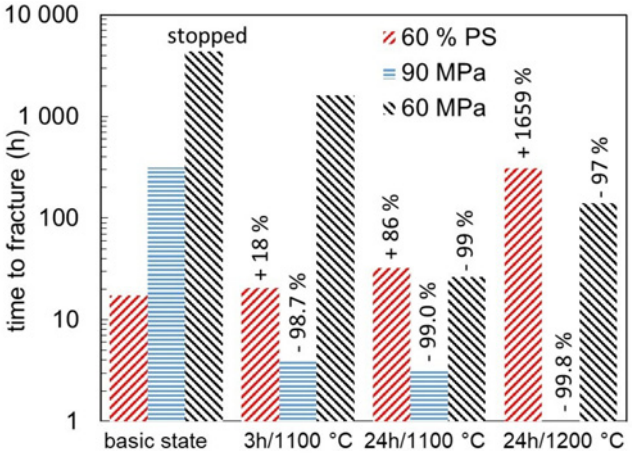

Fig. 4. Influence of the microstructure of the developed Fe-Al-O alloy on time to fracture in dependence on the loading.

summarized in Tables 3 and 4, respectively.

Creep testing under the applied stress of 90 MPa resulted in the failure of all the tested specimens, see Table 3. The highest time to fracture as well as the lowest average secondary creep rate and creep ductility were obtained for the basic state of the material (see Figs. 3c,d). This corresponds to the fact that 90 MPa is only 56 % of the basic state PS. The creep response of all the heat-treated ODS alloys corresponds to their respective tensile properties determined at 800 ℃. In the case of batches heat-treated at 1100 ℃, the loading of 90 MPa was close to the PS (76 % annealed for 3 h and 90 % annealed for 24 h), and in the case of batch heat-treated at 1200 ℃, the value of 90 MPa corresponds almost to its UTS. The heat-treated batches were therefore loaded either close to the onset of plastic deformation (1100 ℃ batches) or in the regime of unstable macroplastic deformation (1200 ℃ batch). Thus, enhanced dislocations mobility in this regime deteriorates any creep resistance, demonstrated by very short times to fracture. Nevertheless, the 1200 ℃ batch showed the highest creep fracture strain due to its largest grain size.

The creep tests at 60 MPa allowed a comparison of the creep behaviour properly as all specimens were loaded safely in the elastic regime of tensile loading. The results are shown in Table 4. The test of the basic state material was stopped after 6 months, even though the specimen did not rupture. The heat-treated batch 24 h/1100 ℃ batch showed the lowest time to fracture, while the other two heat-treated batches showed one or even two orders of magnitude longer times to fracture. The explanation can be given as follows. The dislocations were loaded to the same stress level in all specimens, but their motion was hindered by the different density of obstacles (oxide particles and grain boundaries). The highest obstacle density (i.e., lowest dislocation mobility) was in the basic state and decreased through the 3 h/1100 ℃ and 24 h/1100 ℃ batches to the 24 h/1200 ℃ batch. The grain boundary diffusion was presumably also the highest for the basic state and lowest for the 24 h/1200 ℃ batch, as the number of grain boundaries decreased with heat treatment temperature and time applied. So the dislocations motion in the basic state material was significantly blocked, and creep was effectuated by grain boundary diffusion. As mentioned in [5, 13], the oxide particles act as the attractive obstacles for dislocations, and the stress threshold value has to be overcome to detach dislocations from the at-

Table 3. Creep characteristics of Fe-Al-O ODS alloy states tested under tensile loading of 90 MPa

Specimen	Tensile loading (MPa)	Time to fracture (h)	Average secondary creep rate (h^{-1})	Creep fracture strain (%)
Basic state	90	316.07	4.00×10^{-5}	2.25
3 h/1100 ℃	90	4.07	7.90×10^{-3}	4.37
24 h/1100 ℃	90	3.16	2.56×10^{-2}	9.73
24 h/1200 ℃	90	0.66	2.13×10^{-1}	14.44

Table 4. Creep characteristics of the developed Fe-Al-O alloy tested under tensile loading of 60 MPa

Specimen	Tensile loading (MPa)	Time to fracture (h)	Average secondary creep rate (h^{-1})	Creep fracture strain (%)
Basic state	60	4337.00 – stopped test	3.00×10^{-6}	3.20 – stopped test
3 h/1100 ℃	60	1611.14	9.00×10^{-6}	3.09
24 h/1100 ℃	60	26.41	1.80×10^{-3}	6.28
24 h/1200 ℃	60	140.51	1.00×10^{-4}	2.71

Table 5. The grain size of specimens of Fe-Al-O ODS before and after testing at 800 °C under tensile loading of 60 % of PS

Specimen	Grain size before testing (μm)	Grain size after testing (μm)
Basic state	0.4 ± 0.2	0.35 ± 0.15
3 h/1100 °C	0.4 ± 0.1	0.4 ± 0.1
24 h/1100 °C	0.45 ± 0.2	0.45 ± 0.2
24 h/1200 °C	0.5 ± 0.4 (fine-grained area) 79.7 ± 31.7 (coarse-grained area)	0.7 ± 0.6 58.0 ± 44.5

tracting particles. Since the largest number of the fine particles is present in the basic material state compared to the alloys after heat treatment, the most pronounced dislocation blocking by oxide particles was observed. However, the large number of grain boundaries allows the grain boundary diffusion. In the case of the heat-treated alloy states, the decrease of the obstacles to dislocation motion connected with oxide particles coarsening and the decrease of the grain boundaries related to the grain growth changed the material's response to the creep loading. The 3 h/1100 °C batch combined less restricted dislocation motion with diffusion, leading to a long time to fracture. The 24 h/1100 °C batch possessed the worst combination of dislocations hindering and high grain boundary diffusion, which resulted in the worst resistance to creep. The 24 h/1200 °C batch had the most mobile dislocations (due to the lack of oxide particles obstacles). Still, it significantly decreased the number of grain boundaries that decreased grain boundary diffusion, enhanced creep resistance, and prolonged the time to fracture.

Results of the creep tests performed at 60 % of PS were compared via Larson-Miller criterion according to the formula (1) with data available in the literature [18], Eq. (1):

$$\mathrm{PLM} = T(C + \log t_\mathrm{f}) \times 10^{-3}, \qquad (1)$$

where C is a material-specific constant, t_f is the time to rupture in hours, and T is the temperature in K. Taking into account the Larson-Miller criterion, the creep characteristics obtained for the developer material in the basic state and after heat treatment are lower than those for conventional ODSs, however, better than those for Fe-Al based materials and comparable with properties of Ni-Al and Ti-Al based materials, Fig. 5 [19, 20].

4.2. Microstructural stability

To prove the microstructure stability during the creep loading, EBSD analysis before and after testing was performed. The results are shown in the form of histograms in Fig. 6.

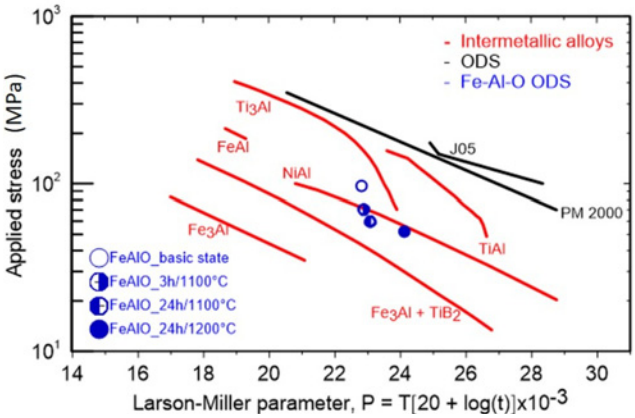

Fig. 5. Comparison of the creep characteristics of the developed Fe-Al-O alloy.

From the obtained results, the microstructure in terms of the grain size can be considered stable during creep loading at 800 °C. The comparison of grain size before and after creep tests revealed only statistically negligible changes. The results are summarized in Table 5.

4.3. Creep damage mechanism

Detailed analysis of the polished specimens of the crept specimens along the loading axes revealed the creep damage mechanism of all the Fe-Al-O ODS alloy batches, see Fig. 7. Only the basic material and batch heat-treated at 1200 °C for 24 h, the extreme cases, are presented here. Except for the stopped specimen (basic state/60 MPa/800 °C), in all of the cases, defects (cavities and cracks) were observed on the polished specimen sections. The size and amount of the defects correspond well to the creep characteristics of the tested materials. Increasing the applied creep stress resulted in an increasing number of defects.

The defects were usually initiated at the grain boundaries and on the matrix/dispersed oxide particle interfaces, which correlates to the basic creep fracture mechanisms [17]. The nucleated defects act as the crack initiation sites; subsequently, the crack's growth is facilitated by the coalescence of the defects, usually

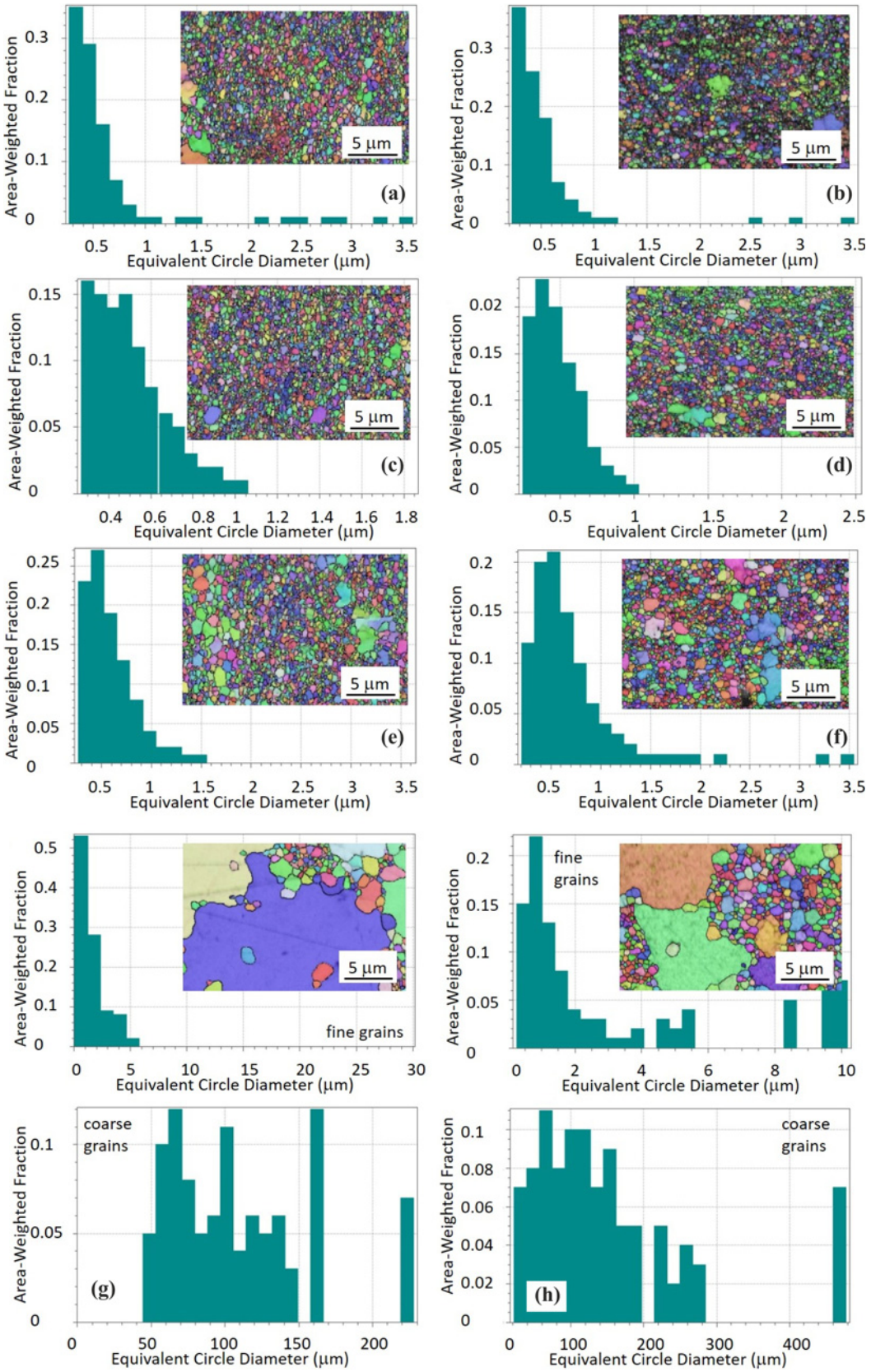

Fig. 6. Grain size histograms of specimens of the developed Fe-Al-O alloy before and after testing at 800 °C under tensile loading of 60 % PS, EBSD: (a) basic state – before testing, (b) basic state, 96.6 MPa, 17.44 h to fracture, (c) 3 h/ 1100 °C – before testing, (d) 3 h/1100 °C, 70.8 MPa, 20.63 h to fracture, (e) 24 h/1100 °C – before testing, (f) 24 h/1100 °C, 60.0 MPa, 32.48 h to fracture, (g) 24 h/1200 °C – before testing, for fine and coarse grains, and (h) 24 h/ 1200 °C, 52.2 MPa, 306.72 h to fracture for fine and coarse grains.

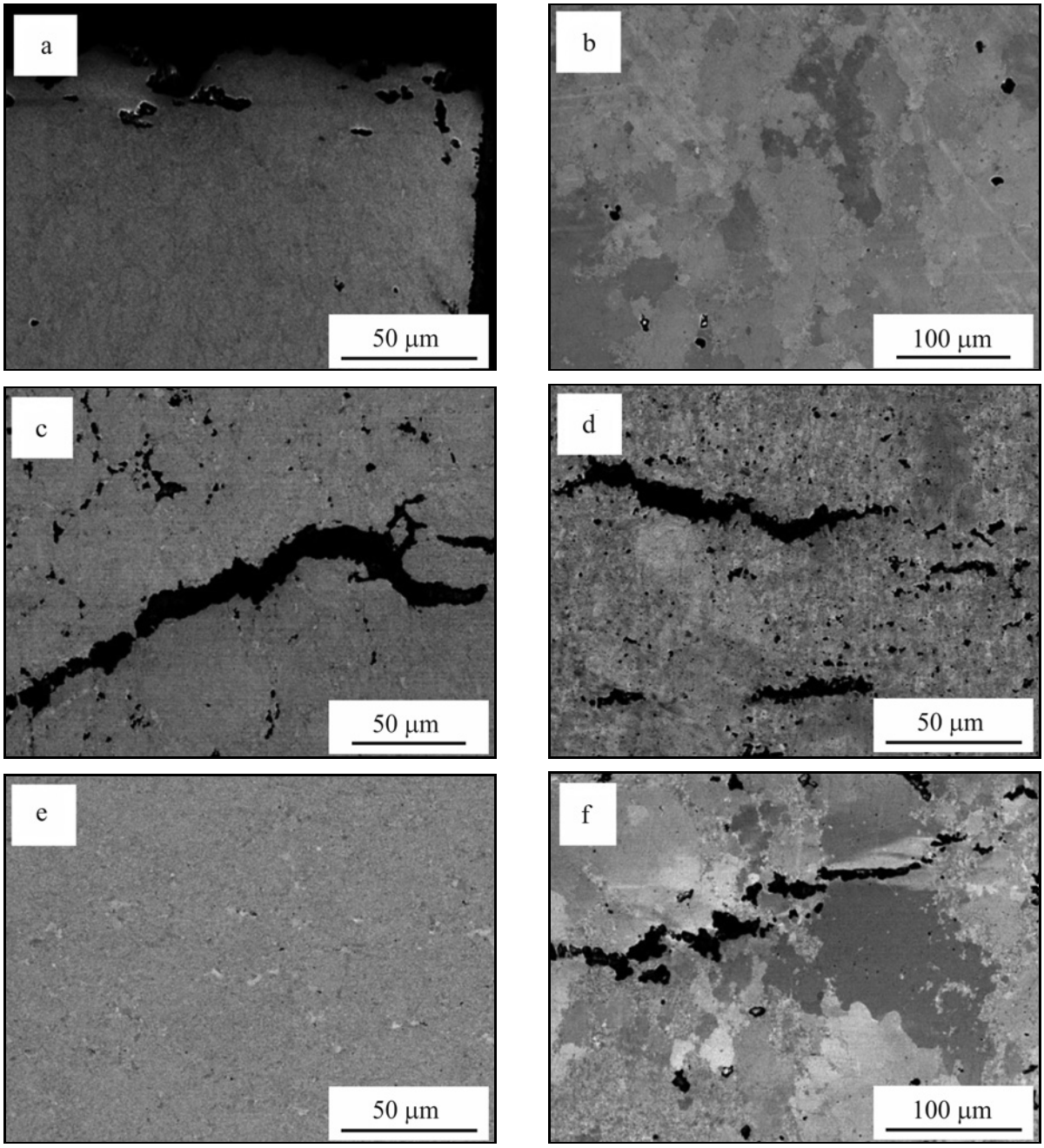

Fig. 7. Creep mechanism of the developed Fe-Al-O alloy tested at 800 °C under loading, SEM, BSE: (a) basic state, 60 % $\sigma_{0.2}$ = 96.6 MPa, 17.44 h to fracture, (b) 24 h/1200 °C, 60% $\sigma_{0.2}$ = 52.2 MPa, 306.72 h to fracture, (c) basic state, 90 MPa, 316.07 h to fracture, (d) 24 h/1200 °C, 90 MPa, 0.66 h to fracture, (e) basic state, 60 MPa, stopped test, (f) 24 h/1200 °C, 60 MPa, 140.51 h to fracture.

along the grain boundaries. Subsequent linking of individual cracks was responsible for specimen failure. The defects were nucleated due to the overcritical loading in most of the cases. Only in several cases (at least for the basic state tested at 60 MPa) only rather seldom diffusion growth mechanism of the isolated creep cavities (first stage of creep damage) can be observed. No specific internal microstructure arrangement was revealed by electron microscopy due to the refined grains and a high amount of finely dispersed particles acting as obstacles for moving dislocations.

When the load 60 % of PS at 800 °C was applied in the creep test, intensive cavity nucleation, growth, and coalescence were observed for the fine-grained batches due to the plastic flow which resulted in a relatively short time to fracture. The cavities acted as the crack initiation sites, and the crack growth was facilitated by the coalescing cavities, see Fig. 7a. In the case of the batch heat-treated at 1200 °C for 24 h, a smaller number of cavities and cracks was observed on the

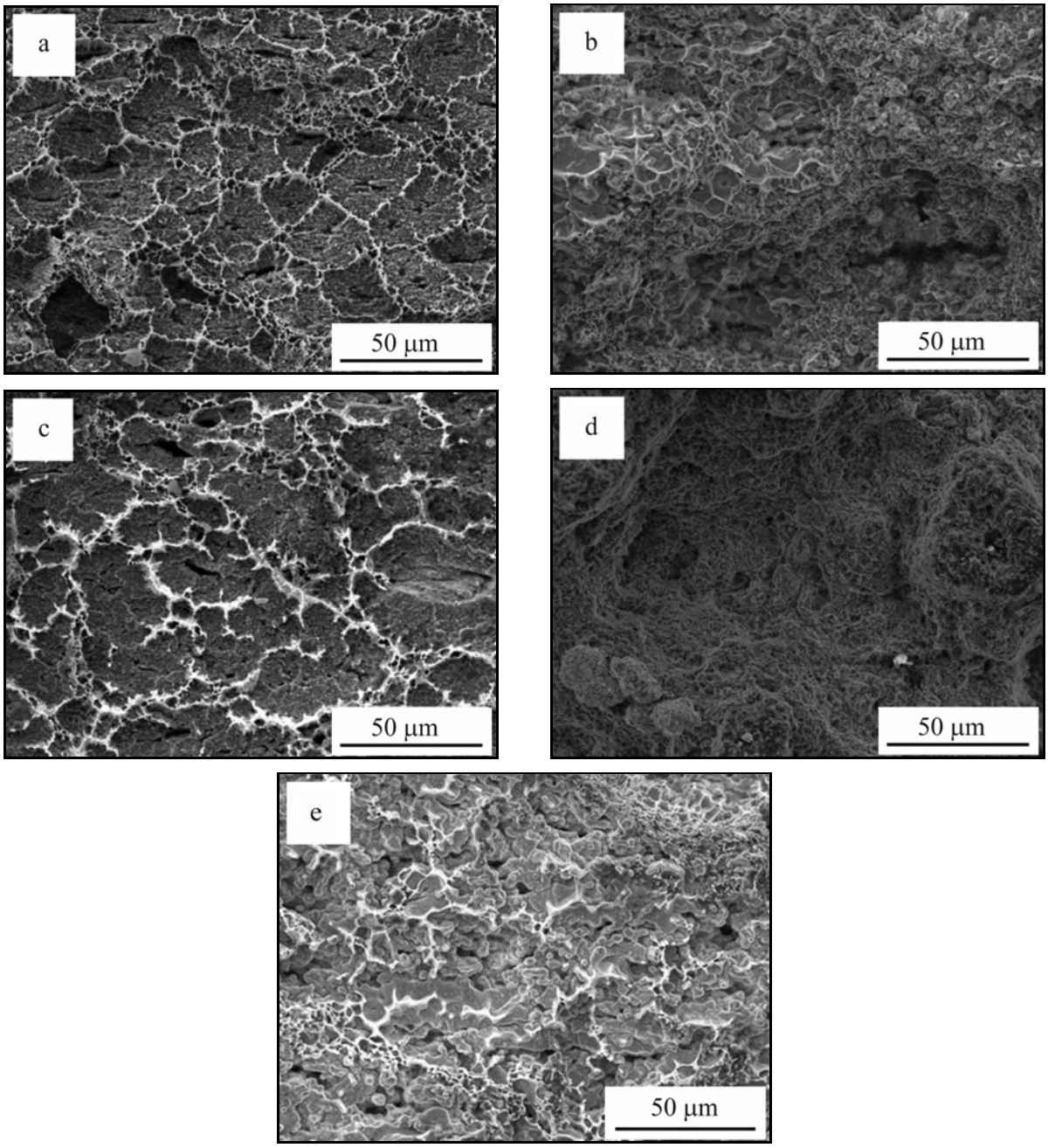

Fig. 8. Fracture surface of specimens of the developed Fe-Al-O alloy tested at 800 °C under tensile loading, SEM: (a) basic state, 60 % $\sigma_{0.2}$ = 96.6 MPa, 17.44 h to fracture, (b) 24 h/1200 °C, 60 % $\sigma_{0.2}$ = 52.2 MPa, 306.72 h to fracture, (c) basic state 90 MPa, 316.07 h to fracture, (d) 24 h/1200 °C, 90 MPa, 0.66 h to fracture, and (e) 24 h/1200 °C, 60 MPa, 140.51 h to fracture; (basic state specimen was not fractured till the end of the test).

polished specimen surface, which can be explained by much lower applied stress corresponding to 60 % of PS and the low number of grain boundaries, see Fig. 7b.

The load of 90 MPa was too high for the heat-treated alloy batches. The value is close to the PS of the batches treated at 1100 °C and the same as the UTS for the batch heat-treated at 1200 °C. Due to extensive plastic deformation, a large number of cavities and cracks resulting in very fast specimen failure were formed during the creep loading. The basic state of material also exhibited many defects acting as the cracks initiation sites, although the applied loading was lower than 60 % of PS. The time to fracture was nearly 500 times higher for the basic state when compared to the heat-treated states; however, a comparable amount of defects was observed in the basic state when compared to the heat-treated batch, see Figs. 7c, d.

The specimen of the alloy's basic state did not break even after 6 months of testing at the applied

load of 60 MPa. No significantly developed defects were observed in the specimen, see Fig. 7e. In the case of the batch heat-treated at 1200 ℃ for 24 h, quite an intensive formation of cavities and cracks was observed. Even though in this case the applied stress of 60 MPa was higher than 60 % of PS and the time to fracture was relatively low, the value of the time to fracture was still higher than for the batch heat-treated at 1100 ℃ for the same time. The difference can be attributed to the bimodal grain size distribution, which could be beneficial in the case of low applied creep stress, see Fig. 7f.

In terms of creep, the fine-grained microstructures are detrimental due to diffusional creep occurring due to matter transport along grain boundaries that overcome the effect of particle strengthening. Thus, creep damage occurs throughout the whole volume, and the fracture process is non-localized.

Defects in the material bulk (cavities and cracks) formed during the creep test observed at the surfaces of the tested specimens (Fig. 7) were visible also at the fracture surface of broken specimens, see Fig. 8.

SEM analysis of the creep fracture surfaces of the broken specimens revealed the creep fracture's characteristic features as the formation of micro-cracks by coalescence of cavities (see Fig. 8). However, no such features were observed on the fracture surface of the specimen heat-treated at 1200 ℃ for 24 h tested under 90 MPa at 800 ℃ due to too short time to fracture (0.66 h). This fracture can be rather considered as a ductile fracture due to dimples nucleated at large oxide particles.

It can be assumed that the cavities nucleated during loading act as the initiation sites for cracks, and their growth and coalescence lead to the formation of cracks responsible for specimen failure. The coalesced cavities are apparent at the basic state's fracture surfaces and the batches heat-treated at 1100 ℃. In the case of the batch heat-treated at 1200 ℃, the fracture surface indicates that the crack propagates along grain boundaries between large grains with a high occupancy of oxides. In case of low applied stress, the fracture occurs by coalescence of cavities created due to the creep loading, see Fig. 8b, while plastic growth of dimples nucleated at large oxides is responsible for the fracture at high applied stress, see Fig. 8d.

5. Conclusions

An advanced Fe-Al-O based alloy was developed and prepared at IPM. Three different regimens of heat treatment were used to modify the material microstructure. Tensile tests performed at 800 ℃ provided basic characteristics utilized for subsequent creep testing of the prepared batches. Based on the results of performed experiments, the following conclusions can be stated:

– creep damage occurs in the whole volume of the material and it is characterized by the growth and coalescence of cavities nucleated at grain boundaries on the dispersed particles,

– the highest dislocation creep resistance is achieved by the strongest hindering of dislocations motion, that can be achieved by small grain size and high number density of dispersed particles, which are the typical features of the basic state material microstructure,

– the highest time to fracture for creep loading at 60 % of PS was achieved by the batch heat-treated at 1200 ℃ for 24 h due to its bimodal coarse-grained; the corresponding 60 % PS loading stress was, however, the lowest among all material's variants,

– heat treatment at 1100 ℃ did not significantly affect creep resistance compared to the basic state od the ODS alloy.

Acknowledgements

The research of M. J., L. S., and J. S. has been funded by the Czech Science Foundation in the frame of the project 17-01641S. The research of S. F, I. K., N. L., and F. Š. has been financially supported by the Ministry of Education, Youth and Sports of the Czech Republic under the project m-IPMinfra (CZ.02.1.01/0.0/0.0/16_013/0001823). The equipment and the base of research infrastructures IMPinfra and CEITEC (LQ1601) were used during the research activities. The authors would like to thank Jan Procházka for careful specimen preparation and EBSD data acquisition.

References

[1] M. Palm, Concepts derived from phase diagram studies for the strengthening of Fe-Al-based alloys, Intermetallics 13 (2005) 1286–1295. doi:10.1016/j.intermet.2004.10.015

[2] I. Kubena, B. Fournier, T. Kruml, Effect of microstructure on low cycle fatigue properties of ODS steels, Journal of Nuclear Materials 424 (2012) 101–108. doi:10.1016/j.jnucmat.2012.02.011

[3] J. H. Lee, Development of oxide dispersion strengthened ferritic steels with and without aluminum, Frontiers in Energy 6 (2012) 29–34. doi:10.1007/s11708-012-0178-x

[4] B. Mašek, O. Khalaj, Z. Nový, T. Kubina, J. Jirkova, J. Svoboda, C. Štádler, Behaviour of new ODS alloys under single and multiple deformation, Materials and Technology 50 (2016) 891–898. doi:10.17222/mit.2015.156

[5] C. Zakine, C. Prioul, D. François, Creep behaviour of ODS steels, Materials Science and Engineering A 219 (1996) 102–108. doi:10.1016/S0921-5093(96)10415-9

[6] E. Ghali, W. Dietzel, K.-U. Kainer, General and localized corrosion of magnesium alloys: A critical review, Journal of Materials Engineering and Performance 13 (2004) 7–23. doi:10.1361/10599490417533

[7] H. Mirzadeh, A. Zomorodian, Grain growth in nanocrystalline iron and Fe-Al alloys, Metals and Materials International 16 (2010) 83–86. doi:10.1007/s12540-010-0083-y
[8] D. Kumar, U. Prakash, V. V. Dabhade, K. Laha, T. Sakthivel, Development of oxide dispersion strengthened (ODS) ferritic steel through powder forging, Journal of Materials Engineering and Performance 26 (2017) 1817–1824. doi:10.1007/s11665-017-2573-2
[9] J. Chao, R. Rementeria, M. Aranda, C. Capdevila, J. L. Gonzalez-Carrasco, Comparison of ductile-to-brittle transition behavior in two similar ferritic oxide dispersion strengthened alloys, Materials 9 (2016) 637. doi:10.3390/ma9080637
[10] D. Bártková, M. Šmíd, B. Mašek, J. Svoboda, F. Šiška, Kinetic study of static recrystallization in an Fe-Al-O ultra-fine-grained nanocomposite, Philosophical Magazine Letters 97 (2017) 379–385. doi:10.1080/09500839.2017.1378445
[11] J. Svoboda, V. Horník, L. Stratil, H. Hadraba, B. Mašek, O. Khalaj, H. Jirková, Microstructure evolution in ODS alloys with a high-volume fraction of nano oxides, Metals 8 (2018) 1079. doi:10.3390/met8121079
[12] D. J. Srolovitz, M. J. Luton, R. Petkovic-Luton, D. M. Barnett, W. D. Nix, Diffusionally modified dislocation-particle elastic interactions, Acta Metallurgica 32 (1984) 1079–1088. doi:10.1016/0001-6160(84)90011-7
[13] E. Arzt, D. S. Wilkinson, Threshold stresses for dislocation climb over hard particles: The effect of an attractive interaction, Acta Metallurgica 34 (1986) 1893–1898. doi:10.1016/0001-6160(86)90247-6
[14] S. Fintová, I. Kuběna, N. Luptáková, M. Jarý, M. Šmíd, L. Stratil, F. Šiška, J. Svoboda, Development of advanced Fe-Al-O ODS alloy microstructure and properties due to heat treatment, Journal of Materials Research 35 (2020) 2789–2797. doi:10.1557/jmr.2020.278
[15] O. Khalaj, H. Jirková, T. Janda, L. Kučerová, T. Studecký, J. Svoboda, Improving the high-temperature properties of a new generation of Fe-Al-O oxide-precipitation-hardened steels, Materiali in tehnologije 53 (2019) 495–504. doi:10.17222/mit.2018.227
[16] M. Auger, T. Leguey, A. Munoz, M. Monge, V. de Castro, P. Fernandez, G. Garces, R. Pareja, Microstructure and mechanical properties of ultrafine-grained Fe-14Cr and ODS Fe-14Cr model alloys, Journal of Nuclear Materials 417 (2011) 213–216. doi:10.1016/j.jnucmat.2010.12.060
[17] J. Pelleg, Creep in Ceramics, Springer International Publishing, New York, 2017. doi:10.1007/978-3-319-50826-9
[18] F. R. Larson, J. Miller, A time-temperature relationship for rupture and creep stresses, Trans. ASME 74 (1952) 765–771.
[19] R. C. Reed, The Superalloys: Fundamentals and Applications, Cambridge University Press, Cambridge, 2008.
[20] G. Korb, M. Rühle, H. P. Martonz, New iron-based ODS-superalloys for high demanding applications, Proceedings of the International Gas Turbine and Aero-engine Congress and Exposition 1991, Code 111471. doi:10.1115/91-GT-405